Article

Cell Reports

Caudal Ganglionic Eminence Precursor Transplants Disperse and Integrate as Lineage-Specific Interneurons but Do Not Induce Cortical Plasticity

Graphical Abstract

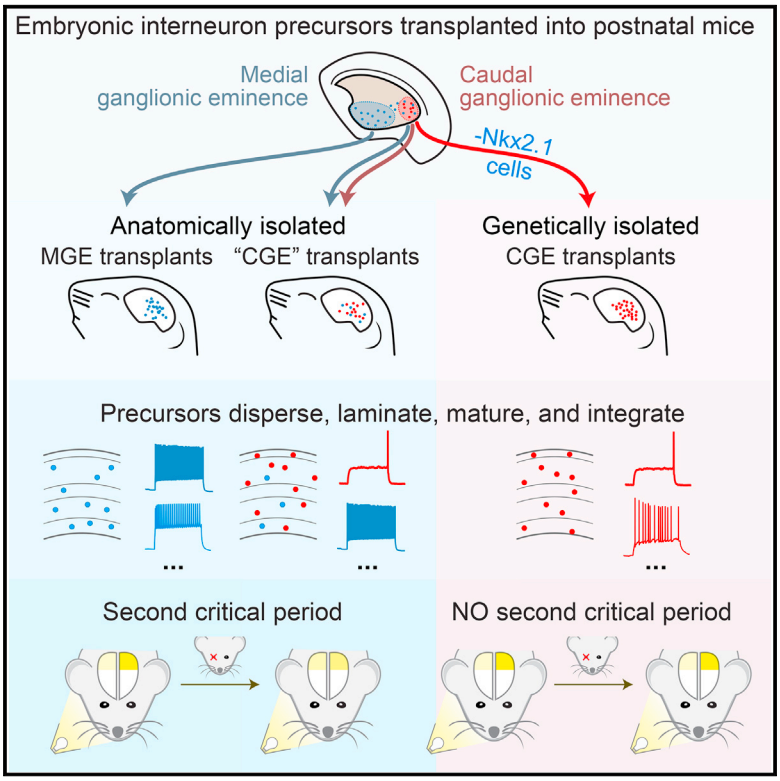

Authors

Phillip Larimer, Julien Spatazza, Juan Sebastian Espinosa, ..., Andrea R. Hasenstaub, Michael P. Stryker, Arturo Alvarez-Buylla

Correspondence

abuylla@stemcell.ucsf.edu

In Brief

Larimer et al. demonstrate successful transplantation of caudal ganglionic eminence (CGE) neuronal progenitors that differentiate into functional interneurons in the postnatal mouse visual cortex. Although CGE transplants induce ocular dominance plasticity, it is mediated by a small fraction of interneurons derived from the medial ganglionic eminence contained in the transplants.

Highlights

- Transplanted CGE-derived neurons migrate and differentiate in the postnatal mouse brain
- Transplanted CGE-derived neurons functionally integrate into local circuits
- CGE transplantation does not reactivate visual cortex plasticity for ocular dominance

Larimer et al., 2016, Cell Reports *16*, 1391–1404
August 2, 2016
http://dx.doi.org/10.1016/j.celrep.2016.06.071

Cell Reports
Article

Caudal Ganglionic Eminence Precursor Transplants Disperse and Integrate as Lineage-Specific Interneurons but Do Not Induce Cortical Plasticity

Phillip Larimer,[1,2,3,8] Julien Spatazza,[4,5,8] Juan Sebastian Espinosa,[1,6,8] Yunshuo Tang,[4,5,8] Megumi Kaneko,[1,6] Andrea R. Hasenstaub,[1,3,7,9] Michael P. Stryker,[1,6,9] and Arturo Alvarez-Buylla[4,5,9,*]
[1]Center for Integrative Neuroscience, University of California, San Francisco, 675 Nelson Rising Lane, San Francisco, CA 94158, USA
[2]Department of Neurology, University of California, San Francisco, San Francisco, CA 94143, USA
[3]Coleman Memorial Laboratory, University of California, San Francisco, San Francisco, CA 94158, USA
[4]Department of Neurological Surgery, University of California, San Francisco, San Francisco, CA 94143, USA
[5]The Eli and Edythe Broad Center of Regeneration Medicine and Stem Cell Research, University of California, San Francisco, San Francisco, CA, 94143, USA
[6]Department of Physiology, University of California, San Francisco, San Francisco, CA 94143, USA
[7]Department of Otolaryngology-Head and Neck Surgery, University of California, San Francisco, San Francisco, CA 94143, USA
[8]Co-first author
[9]Co-senior author
*Correspondence: abuylla@stemcell.ucsf.edu
http://dx.doi.org/10.1016/j.celrep.2016.06.071

SUMMARY

The maturation of inhibitory GABAergic cortical circuits regulates experience-dependent plasticity. We recently showed that the heterochronic transplantation of parvalbumin (PV) or somatostatin (SST) interneurons from the medial ganglionic eminence (MGE) reactivates ocular dominance plasticity (ODP) in the postnatal mouse visual cortex. Might other types of interneurons similarly induce cortical plasticity? Here, we establish that caudal ganglionic eminence (CGE)-derived interneurons, when transplanted into the visual cortex of neonatal mice, migrate extensively in the host brain and acquire laminar distribution, marker expression, electrophysiological properties, and visual response properties like those of host CGE interneurons. Although transplants from the anatomical CGE do induce ODP, we found that this plasticity reactivation is mediated by a small fraction of MGE-derived cells contained in the transplant. These findings demonstrate that transplanted CGE cells can successfully engraft into the postnatal mouse brain and confirm the unique role of MGE lineage neurons in the induction of ODP.

INTRODUCTION

Inhibitory interneurons are important regulators of cortical function and plasticity (Hensch, 2005). Ocular dominance plasticity (ODP), in which monocular visual deprivation during a brief juvenile critical period leads to marked changes in the relative strength of binocular visual cortical responses to ipsilateral versus contralateral visual inputs, provides a unique paradigm for studying the role of inhibition in behavioral plasticity. Cortical inhibitory neurons are a genetically, anatomically, and physiologically diverse group of cells with numerous functions posited in sensory processing, timing precision, learning, and behavior (reviewed in Fishell and Tamás, 2014). Developmental studies have demonstrated that (1) perisomatic inhibition from parvalbumin (PV)-expressing interneurons matures during the critical period (Chattopadhyaya et al., 2004); (2) degradation of the extracellular matrix preferentially surrounding the terminals of PV fast-spiking interneurons heightens ODP (Pizzorusso et al., 2002); and (3) fast-spiking PV interneuron synapses onto principal neurons potentiate following monocular deprivation (MD) during the critical period (Maffei et al., 2006). These results suggest a key role for PV interneurons in the induction of ODP. Consistent with this, juvenile-like ODP is reactivated by heterochronic transplantation of medial ganglionic eminence (MGE) interneuron precursors (Southwell et al., 2010), which develop into several interneuron subtypes including PV-expressing interneurons. However, recent work has demonstrated that PV interneurons are not unique in this regard: heterochronic transplantation and maturation of somatostatin (SST)-expressing neurons, another MGE-derived population, also reactivates juvenile-like ODP (Tang et al., 2014). This raises the question of whether young interneurons are, in general, capable of reopening sensory critical periods. Alternatively, the ability to re-open ODP could be specific to certain types of interneurons.

The vast majority of cortical interneurons originate either from the MGE or from the caudal ganglionic eminence (CGE; Wonders and Anderson, 2006). CGE-derived neurons account for 30% of inhibitory neurons in the mouse cortex (Nery et al., 2002) and are anatomically and functionally distinct from MGE-derived neurons. Whether CGE-derived interneurons have the potential to induce ODP remains unknown. Generating CGE transplants devoid of any MGE cells is complicated as some MGE-derived interneurons migrate through the CGE (Butt et al., 2005). Here, we use a genetic approach to label and/or ablate MGE-derived

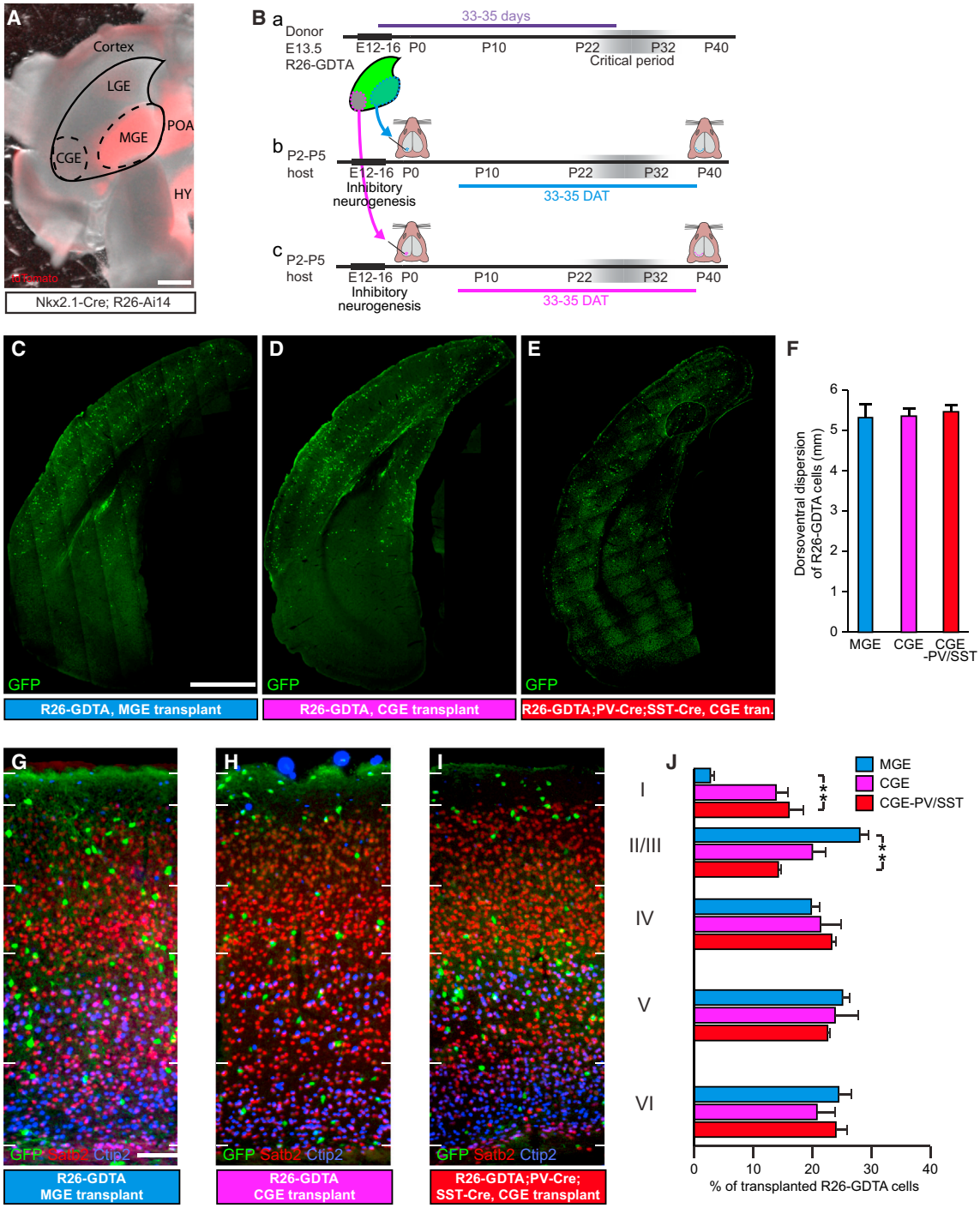

Figure 1. MGE and CGE Transplants Disperse Broadly in Neocortex and Demonstrate Laminar Distributions Consistent with Their Lineages

(A) Anatomical positions of MGE and CGE in E13.5 *Nkx2.1-Cre;R26-Ai14* mouse brain (tdTomato expression recapitulates Nkx2.1 expression pattern and is shown here to demonstrate the spatial extent of MGE lineage neurons but was not used to guide dissection). Scale bar, 500 μm. POA, preoptic area; HY, hypothalamus.

(B) Cells were dissected from the MGE or CGE at E13.5 (a), dissociated, and transplanted into the visual cortex of P2–5 hosts. MGE (b) or CGE (c) transplant recipient brains were examined at 33–35 DAT.

(C–E) Coronal brain sections stained for GFP at 35 DAT to detect cells from anatomically isolated MGE (*R26-GDTA* donors; C), anatomically isolated CGE (*R26-GDTA* donors; D), or genetically isolated CGE (*PV-Cre;SST-Cre;R26-GDTA* donors; E) transplants. Scale bar, 1 mm.

(F) Dorsoventral dispersion in the host cortex at 35 DAT of cells from anatomically isolated MGE (blue, n = 5 mice), anatomically isolated CGE (magenta, n = 5 mice), and genetically isolated CGE (red, n = 4 mice) transplants. Error bars represent SEM p = 0.44 by Kruskal-Wallis test.

(legend continued on next page)

cells in CGE grafts. We show that CGE cells migrate, differentiate, and functionally integrate into the host tissue. Transplanted CGE cells receive synaptic contacts from, and make synaptic contacts onto, host neurons and also respond to visual stimulation. Despite this successful engraftment, we find that CGE transplants do not induce ODP unless they contain MGE-derived PV and SST cells.

RESULTS

CGE-Transplant-Derived Cells Disperse in the Host Cortex

We sought to establish whether CGE-derived cells can migrate when heterochronically transplanted into the cortex of neonatal mice and determine how this transplant compares to the well-established dispersal of MGE-derived cells (Alvarez-Dolado et al., 2006; Bráz et al., 2012; Hunt et al., 2013; Martínez-Cerdeño et al., 2010; Wichterle et al., 1999; Zipancic et al., 2010). We transplanted fluorescently labeled precursors from either the MGE or the CGE of E13.5 *R26-GDTA* (Ivanova et al., 2005) donor embryos just medial and lateral to the visual cortex of postnatal day (P) 7 wild-type (C57B6/J) hosts (Figure 1B). The *R26-GDTA* allele facilitates identification of donor cells (through GFP expression) and allows ablation of specific cell types (through diphtheria toxin alpha subunit expression in a Cre-dependent manner). For all CGE transplants, we minimized potential MGE contamination anatomically by dissecting the caudal-dorsal CGE (Figure 1A).

We compared the dorsoventral and laminar dispersion of MGE transplant-derived cells at 35 DAT (days after transplantation, the time at which the plasticity induced by MGE transplantation is maximal) to that of anatomically isolated CGE transplant-derived cells at the same age. Consistent with previous results (Southwell et al., 2010; Tang et al., 2014), we found that E13.5 MGE cells disperse widely after transplantation (Figure 1C) and by 35 DAT have established a preference for deeper cortical layers consistent with their lineage (Figures 1G and 1J; Rudy et al., 2011). CGE cells similarly migrated extensively throughout the cortex after transplantation (Figure 1D), traveling as far as 4.5 mm rostrally from the injection site (data not shown). We quantified the dorsoventral dispersion of transplanted cells and found no difference between MGE and CGE recipient animals (Figure 1F; MGE, 5.3 ± 0.4 mm; CGE, 5.4 ± 0.2 mm; $p > 0.05$ by Kruskal-Wallis test).

We next investigated the laminar organization of transplanted cells in host visual cortex by using immunostaining for the transcription factors Satb2 and Ctip2 to delineate cortical layers (Figures 1G–1I; Figure S1): *Satb2* is preferentially expressed by layer II/III and V neurons (Britanova et al., 2008), while *Ctip2* expression is largely absent in layers II–IV (Arlotta et al., 2005). At 35 DAT, we found that layer I contained a greater fraction of CGE transplant-derived neurons, compared to MGE transplant-derived neurons (Figure 1J; MGE, 2.7% ± 0.6%; CGE, 13.8% ± 2.0%; $p < 0.001$ using Bonferroni-corrected t tests), which is consistent with prior studies showing that CGE is the main source of layer I interneurons (Miyoshi et al., 2010; Rudy et al., 2011). By contrast, a greater fraction of MGE transplant-derived cells was observed in layer II/III (Figure 1J; MGE, 28.1% ± 1.5%; CGE, 20.0% ± 2.3%; $p < 0.05$ using Bonferroni-corrected t tests), while the fraction of transplanted cells in other cortical layers was similar between CGE and MGE transplants (Figure 1J; $p > 0.05$ using Bonferroni-corrected t tests). Taken together, these results demonstrate that transplanted CGE cells in juvenile mouse visual cortex migrate, disperse, and adopt a lamination normal for their lineage. These findings in juvenile mice are in stark contrast with a recent report indicating poor dispersal and aberrant accumulation of transplanted CGE cells in the deep layers of the adult mouse visual cortex (Davis et al., 2015).

CGE-Transplant-Derived Neurons Express Known Markers of Their Lineage

During embryogenesis, MGE and CGE progenitor cells give rise to biochemically distinct subtypes of cortical interneurons. While MGE cells produce large numbers of PV- and SST-expressing interneurons (Anderson et al., 1997; Wichterle et al., 2001), CGE progenitors generate large numbers of RLN (*Reln*, Reelin), VIP (*Vip*, Vasoactive Intestinal Polypeptide), and CR interneurons (*Calb2*, Calretinin) (Lee et al., 2010; Miyoshi et al., 2010). To characterize the molecular identity of neurons derived from either MGE or CGE heterochronic transplants, we immunostained coronal sections of MGE or CGE transplant recipient visual cortex for known markers of MGE and CGE lineage interneurons at 35 DAT (Figures 2A–2H). While the proportions of NPY (*Npy*, Neuropeptide Y; Figure 2C)-expressing cells were similar in MGE and CGE transplants (Figure 2H; MGE, 15.4% ± 4.2%; CGE, 13.3% ± 1.0%; n = 3 mice for each type of transplant; Bonferroni-corrected t test $p > 0.05$), we found significantly more transplanted cells expressing CR (Figures 2A and 2H; MGE, 4.0% ± 0.2%; CGE, 18.8% ± 3.3%; $p < 0.01$), VIP (Figures 2D and 2H; MGE, 0.5% ± 0.5%; CGE, 21.8% ± 2.1%; $p < 0.001$), and RLN (Figures 2E and 2H; MGE, 24.1% ± 1.0%; CGE, 40.5% ± 3.3%; $p < 0.01$) in the visual cortex of CGE recipients (Figure 2H; n = 3 mice for each type of transplant; Bonferroni-corrected t tests), consistent with prior CGE lineage tracing experiments (Lee et al., 2010; Miyoshi et al., 2010). In agreement with the large proportion of PV and SST interneurons generated by MGE progenitors, we found that the majority of the cells derived from our MGE transplants were positive for PV or SST (Figure 2H; PV, 43.6% ± 4.8%; SST, 34.9% ± 2.4%). However, we also observed that a fraction of interneurons generated from anatomically isolated CGE expressed PV or SST (Figures 2F–2H; PV, 9.7% ± 1.5%; SST, 8.2% ± 0.7%).

PV and SST Neurons in CGE Transplants Are Derived from MGE

The presence of interneurons expressing PV and SST in our anatomically isolated CGE transplants (Figures 2F–2H) is inconsistent with prior work demonstrating near exclusion of

(G–I) Mouse brain sections co-stained for GFP, Satb2, and Ctip2 to reveal lamination of cells from anatomically isolated MGE (G), anatomically isolated CGE (H), and genetically isolated CGE (I) transplants at 35 DAT in the host visual cortex. Scale bar, 100 μm.

(J) Proportion of cells from anatomically isolated MGE (n = 5 mice), anatomically isolated CGE (n = 3 mice), and genetically isolated CGE (n = 3 mice) transplants found in each layer of the host visual cortex at 35 DAT. Error bars represent SEM. Significance calculated using Bonferroni-corrected t tests.

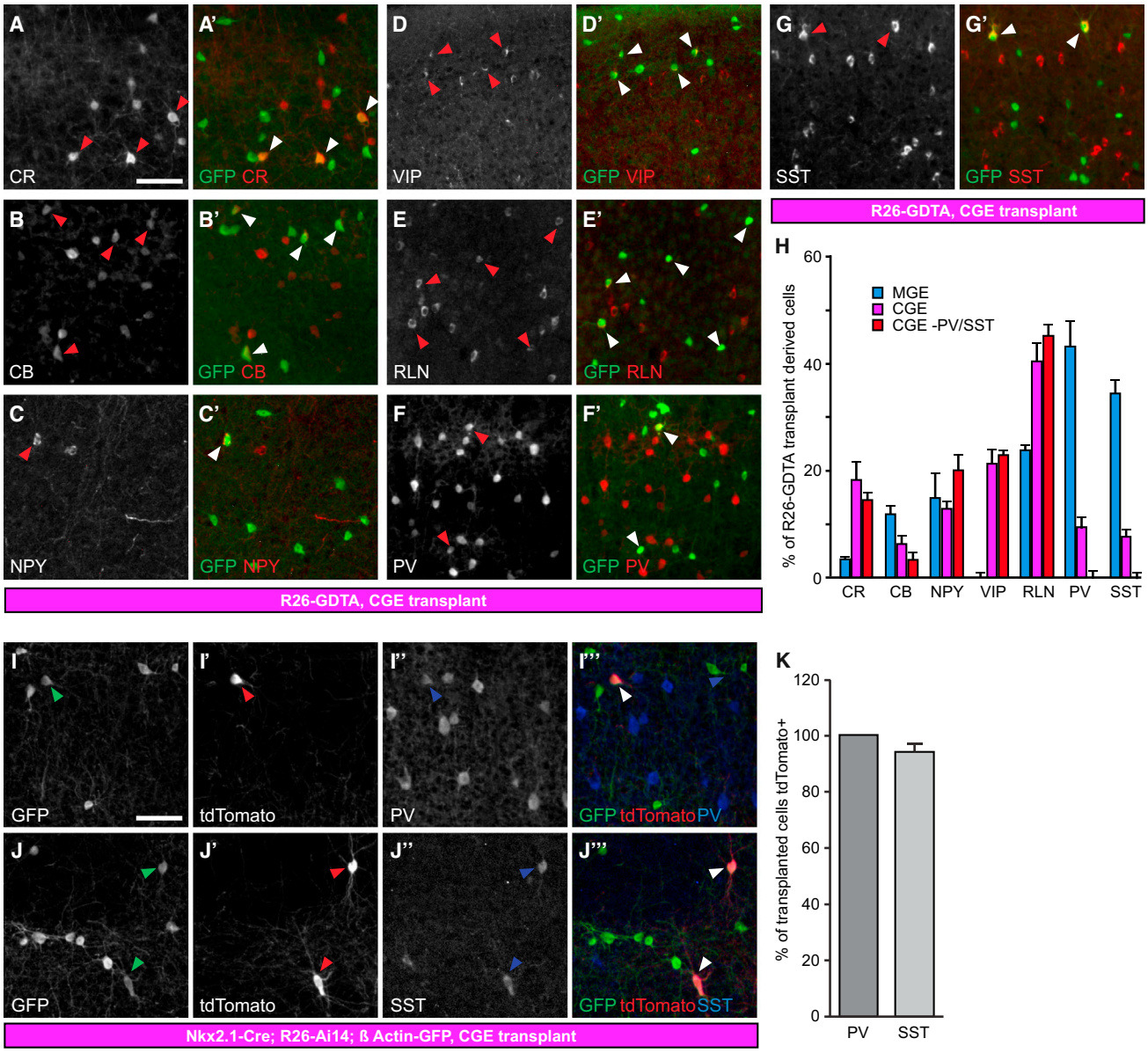

Figure 2. PV and SST Neurons in CGE Transplants Are MGE Derived

(A–G) Visual cortex coronal sections of CGE transplant recipients at 35 DAT stained for GFP (A′–G′), CR (A and A′), CB (B and B′), NPY (C and C′), VIP (D and D′), RLN (E and E′), PV (F and F′), and SST (G and G′). Arrowheads identify double-labeled cells. Scale bar, 100 μm.

(H) Percentage of transplanted GFP$^+$ neurons immunoreactive for subtype markers in (A)–(G) found in *R26-GDTA* MGE (n = 3 mice), *R26-GDTA* CGE (n = 5 mice), and *PV-Cre;SST-Cre;R26-GDTA* CGE (n = 3 mice) recipients at 35 DAT. Error bars represent SEM. Significance calculated using Bonferroni-corrected t tests.

(I) GFP, tdTomato, and PV staining at 35DAT illustrating the presence of *Nkx2.1* lineage PV interneurons in CGE transplants. Arrowheads identify triple-labeled cells. Scale bar, 100 μm.

(J) GFP, tdTomato, and SST staining at 35 DAT as in (I).

(K) Percentage of transplanted PV and SST interneurons which express tdTomato in anatomically isolated CGE transplants. Error bars represent SEM (n = 3 mice).

these markers from CGE-derived interneurons (Lee et al., 2010; Miyoshi et al., 2010; Nery et al., 2002). This could be due to the migration of MGE-derived cells through the CGE en route to caudal cortex (Butt et al., 2005) or could reveal a previously unidentified population of CGE-derived PV- and SST-expressing neurons. To address this issue, we used *Nkx2.1-Cre* (Xu et al., 2008) to investigate whether our CGE transplants contain MGE-derived cells. *Nkx2.1* is a transcription factor required for the development of MGE (Sussel et al., 1999) that is expressed in neurons of the MGE but excluded from the CGE lineage (Figure 1A; Xu et al., 2008). We prepared donor embryos expressing GFP ubiquitously and tdTomato (Madisen et al., 2010) under the

control of *Nkx2.1* (*Nkx2.1-Cre;R26-Ai14;β-actin-GFP*) and transplanted CGE cells anatomically isolated from these embryos into the visual cortex of P5 hosts. At 35 DAT, we found that virtually all the PV- and SST-expressing neurons in our anatomically isolated CGE transplants were also positive for tdTomato (Figures 2I–2K; PV, 100% ± 0%; SST, 94.1% ± 5.1%), thus demonstrating their MGE origin.

To obtain genetically purified transplants of CGE-lineage precursors, we ablated MGE-derived PV and SST cells in our CGE transplants by crossing R26-GTDA mice with mice in which Cre is expressed under the control of both the parvalbumin (Hippenmeyer et al., 2005) and somatostatin (Taniguchi et al., 2011) promoters (*R26-GDTA;PV-Cre;SST-Cre*). Using these mice as donors, we found that our CGE transplants contained virtually no PV and SST neurons at 35 DAT (Figure 2H; PV, 0.5% ± 0.1%; SST, 0.2% ± 0.2%). Apart from the lack of PV and SST interneurons in these genetically purified CGE transplants (referred to below as CGE-PV/SST), no significant differences were found between the interneuron compositions of our two types of CGE transplants. In the CGE-PV/SST transplant recipients, a greater portion of transplanted cells expressed CR, VIP, and RLN compared to interneurons derived from MGE transplants (Figure 2H; CR, 14.9% ± 1.0%; VIP, 23.2% ± 0.5%; RLN, 45.4% ± 1.8%; $p < 0.001$ Bonferroni-corrected t tests), consistent with prior CGE-lineage tracing experiments (Lee et al., 2010; Miyoshi et al., 2010). CB (*Calb1*, Calbindin, Figures 2B and 2H) expression was significantly lower in both types of CGE transplants (Figures 2B and 2H; MGE, 12.3% ± 1.2%; CGE, 6.7% ± 1.3%; CGE-PV/SST, 3.5% ± 1.0%; Bonferroni-corrected t tests). NPY neurons, which originate from both the MGE and the CGE (Butt et al., 2005), were found in similar proportions in our three types of transplants (Figures 2C and 2H).

Migration and lamination were also evaluated for our CGE-PV/SST transplants, which showed similar dorsoventral dispersion to that of anatomically isolated MGE and CGE transplants (Figures 1E and 1F; 5.7 ± 0.2 mm; $p > 0.05$ by Kruskal-Wallis test) and lamination reminiscent of that of anatomically isolated CGE transplants, with larger numbers of cells migrating to layer I and a compensatory decrease in the portion of cells migrating to layer II/III (Figures 1I and 1J; Figure S1; layer I, 16.0% ± 2.5%; layer II/III, 14.2% ± 0.4%). SST-positive Martinotti cells project to layer I where they synapse on the apical dendrites of pyramidal neurons (Gibson et al., 1999; Kawaguchi and Kubota, 1997; Ma et al., 2006; Reyes et al., 1998). Consistent with the depletion of SST cells, we observed a dramatic decrease in the density of GFP fibers in layer I (Figure 1I) of the CGE-PV/SST transplants. In all three preparations (MGE, CGE, and CGE-PV/SST), the overall density of transplant-derived neurons in the host primary visual cortex at 35 DAT was similar, illustrating similar engraftment of all three types of transplant (MGE, 119 ± 9; CGE, 107 ± 4; CGE-PV/SST, 107 ± 9 transplant-derived neurons per mm^2; n = 4, 5, 4 mice, respectively; $p = 0.43$ by ANOVA).

While RLN-expressing neurons represent a significant proportion of transplant-derived neurons in both MGE and CGE transplant recipients, prior work has shown that CGE-derived neurons in layer I preferentially express RLN (Miyoshi et al., 2010) and that CGE-derived RLN neurons do not coexpress SST (Lee et al., 2010). By contrast, MGE-derived RLN-expressing neurons are less prevalent in layer I and preferentially express SST. Accordingly, while 20% ± 3% of transplanted RLN cells were found in cortical layer I of recipients of anatomically isolated CGE transplants, MGE transplant-derived RLN cells systematically avoided layer I (1.7% ± 0.4%; Figures S2A–S2C; n = 4 mice for each type of transplant; t test $p < 0.001$). Additionally, while 80% ± 3% of MGE-derived RLN cells co-expressed SST, only 11% ± 2% of RLN cells in our anatomically isolated CGE transplants coexpressed SST (Figures S2D–S2F; n = 4 mice for each type of transplant; t test $p < 0.001$). Together these results indicate that the RLN cells derived from MGE and CGE transplants represent distinct subclasses of interneurons with distinct biochemical signatures and lamination that are not altered by heterochronic maturation. Many CGE transplant-derived RLN cells also have a typical neurogliaform morphology (Figure S3), consistent with the majority of CGE lineage RLN neurons (Miyoshi et al., 2010).

CGE Transplanted Cells Demonstrate Intrinsic Physiology Typical for Their Lineage

Our lamination and marker expression results suggest that transplanted CGE cells develop according to their pre-transplant fate. To test whether the electrophysiological properties of CGE transplant-derived neurons are also typical of their lineage (Lee et al., 2010; Miyoshi et al., 2010), we used intracellular recordings at 35 DAT. We generated acute brain slices from animals transplanted with a combination of MGE and CGE cells from *Nkx2.1-Cre;R26-Ai14;β-actin-GFP* E13.5 donor embryos, allowing us to compare intrinsic properties of age-matched MGE transplant-derived (GFP^+, $tdTomato^+$) and CGE transplant-derived (GFP^+, $tdTomato^-$) neurons (Figure 3A). When classified according to the Petilla convention (Ascoli et al., 2008), roughly half of transplant-derived MGE lineage neurons were found to be fast spiking (Figure 3Ba; n = 15 of 28 neurons), and the remainder showed a continuous adapting-firing phenotype (Figure 3Bb; n = 13 of 28 neurons).

In contrast, previous studies of CGE-derived neurons have shown a wide variety of electrophysiological properties (Lee et al., 2010; Miyoshi et al., 2010). The electrophysiology of our transplant-derived CGE lineage neurons, either from *VIP-Cre;Ai14* (n = 6 cells from four mice; orange in Figures 3C–3H; Taniguchi et al., 2011), from *Nkx2.1-Cre;R26-Ai14;β-actin-GFP* (n = 11 cells from eight mice; red in Figures 3C–3H), or from *Nkx2.1-Cre;R26-GDTA* (n = 11 cells from seven mice; red in Figures 3C–3H), was similarly quite diverse (Figure 3C) in both passive (Figure 3E) and active (Figures 3F–3H) properties. We found a preponderance (14 of 28 neurons) of continuously adapting neurons (Figure 3Ca), which had a broad range of input resistances (range 0.061–0.801 GΩ; Figure 3E) and afterhyperpolarization (AHP) depths (range 1.6–20.1 mV, Figure 3G). The second most common spiking phenotype was burst non-adapting non-fast spiking (Figure 3Cb) with other phenotypes (Figures 3Cc–3Ch) being less common.

The majority of CGE neurons differentiate into either RLN-expressing neurogliaform cells of the superficial laminae or VIP-expressing neurons. To address whether VIP-expressing neurons derived from CGE transplants demonstrated spiking patterns consistent with those previously observed (Lee et al., 2010),

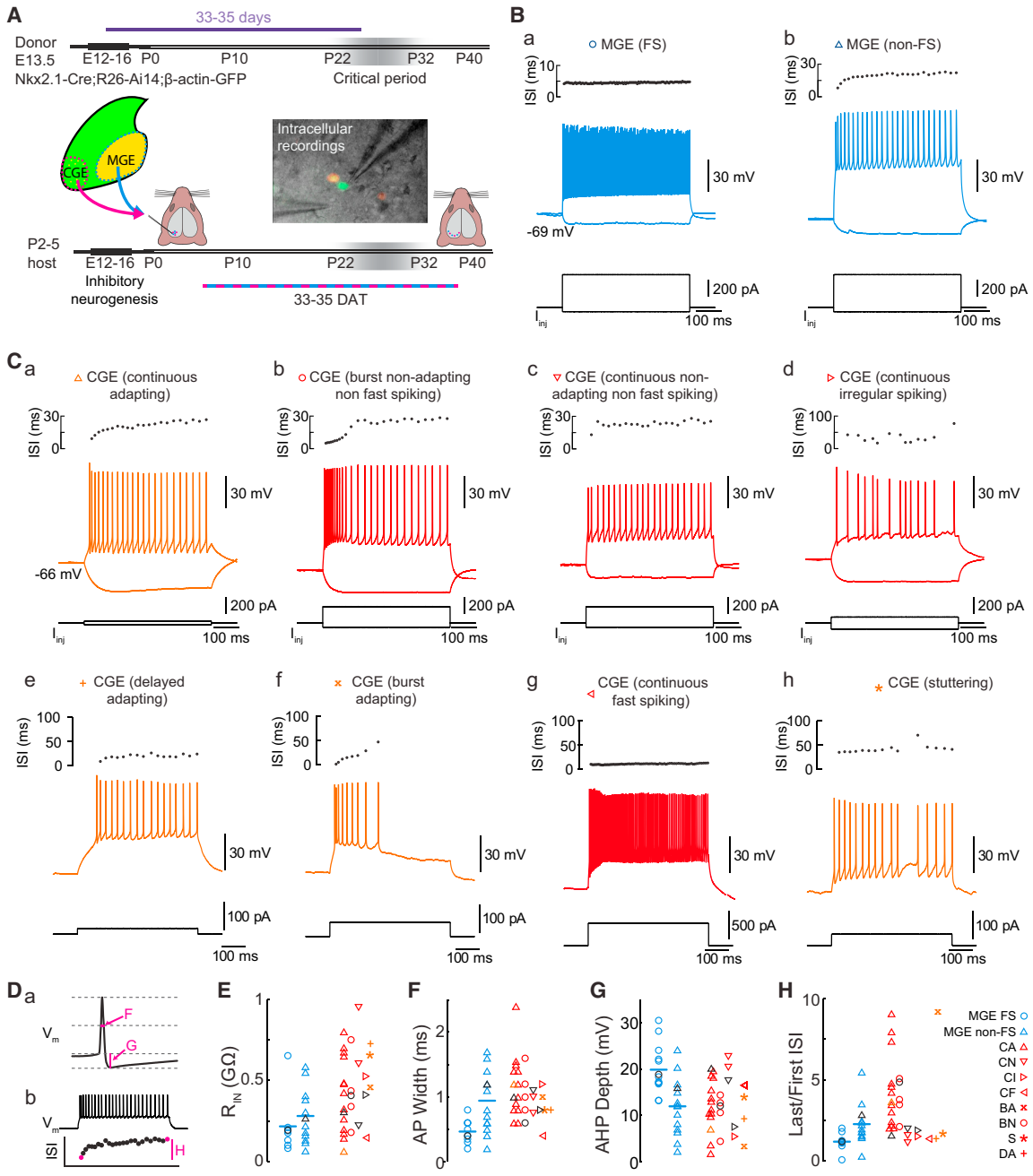

Figure 3. Heterochronically Transplanted Interneuron Precursors Develop Diverse Electrophysiological Phenotypes

(A) MGE and CGE cells from donor mice expressing GFP ubiquitously and tdTomato specifically in MGE lineage neurons (*Nkx2.1-Cre;R26-Ai14;β-actin-GFP*) or tdTomato exclusively in VIP neurons (*VIP-Cre;R26-Ai14*) were harvested at E13.5 and transplanted into visual cortex of P2–7 hosts. Intracellular recordings from slices prepared at ~35 DAT evaluate intrinsic physiological properties of transplant-derived interneurons. Infrared spectroscopy-differential interference contrast (IR-DIC) video micrograph with overlaid fluorescence shows a CGE-derived neuron (GFP only) and an MGE-derived neuron (GFP^+, $tdTomato^+$).

(B) Example voltage (center) and interspike interval (ISI) responses (top) from a FS (a) and a non-FS (b) MGE transplant-derived neurons, to hyperpolarizing and depolarizing current injections.

(C) Example voltage (center) and ISI (top) responses of the electrophysiological phenotypes observed among transplant-derived CGE lineage neurons.

(D) Example action potential (a) and firing response (b) to a 500-ms depolarizing current injection demonstrate definitions used for (F)–(H).

(E–H) Input resistance (E), AP width at half maximum (F), AP afterhyperpolarization depth (G), and AP accommodation (H) for MGE transplant-derived (blue) FS (circles) and non-FS (triangles), and CGE transplant-derived (red for GFP^+/$tdTomato^-$ neurons in dual transplants, orange for VIP-Cre expressing) interneurons. Cell type legend at right: CA, continuous adapting; CN, continuous non-adapting non-FS; CI, continuous irregular spiking; CF, continuous fast spiking; BA, burst-adapting; BN, burst non-adapting non-FS; S, stuttering; DA, delayed adapting; after Ascoli et al. [2008]). Black symbols correspond to cells in (B) and (Ca)–(Cd).

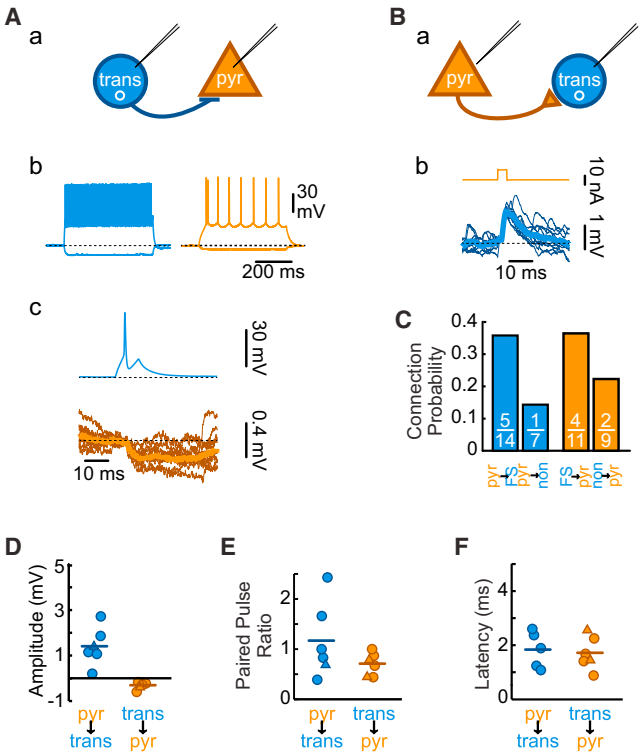

Figure 4. MGE Transplant-Derived Interneurons and Host Pyramidal Neurons Form Frequent Synaptic Connections

(A) Paired recordings from a transplanted MGE lineage fast-spiking interneuron (b, blue) and a host pyramidal neuron (brown) at 35 DAT reveal postsynaptic inhibitory responses (c, brown) to action potentials in the interneuron (c, blue).

(B) Loose patch recordings at 33 DAT of a pyramidal neuron (brown) and an MGE lineage transplanted fast-spiking neuron (blue, intracellular) reveal postsynaptic excitatory responses (b, blue) to current delivery through the loose patch electrode (b, brown).

(C) Summary data of the likelihood that a pyramidal cell connects to an *Nkx2.1-Cre;R26-Ai14* neuron (left) or the reverse (right). White text: number of observed connections (top) versus number of connections tested (bottom).

(D) Quantification of amplitudes of EPSPs (blue) from host pyramidal neurons onto transplant-derived MGE lineage interneurons and IPSPs (with postsynaptic neuron at −60 mV) of transplant-derived neuron onto host pyramidal neuron. Circles indicate that the transplant-derived interneuron in the paired recording had a fast spiking firing pattern; triangles indicate that the transplant-derived interneuron was non-fast spiking.

(E) Quantification of paired-pulse ratios (50-ms interpulse interval) of postsynaptic response amplitudes.

(F) Quantification of latency from action potential to PSP onset.

we used *VIP-Cre;R26-Ai14* donor tissue. We found cells with a continuously adapting phenotype (Figure 3Ca, left), as well as delayed adapting (Figure 3Ce), burst adapting (Figure 3Cf), and stuttering phenotypes (Figure 3Ch), consistent with the diversity seen in prior studies (Prönneke et al., 2015). Previous characterization of CGE lineage RLN-expressing neurons demonstrated that those neurons are commonly late spiking at rheobase (Miyoshi et al., 2010). We found that this was also true in our transplant-derived layer I neurogliaform neurons (time to spike onset for 500-ms step at rheobase: 288 ± 64 ms; n = 6 cells in two animals; Figure S4) further suggesting a preservation of physiological phenotype in the heterochronic environment.

The narrow action potentials and lower input resistance seen in the fast-spiking MGE transplant-derived neurons are also typical for the predominant class of neurons of the MGE lineage (Butt et al., 2005; Miyoshi et al., 2010; Southwell et al., 2010), demonstrating that both CGE and MGE transplant-derived cells are electrically active following transplantation and develop electrophysiological phenotypes similar to those of endogenous mature interneurons. Curiously, we found among our CGE transplanted neurons a single cell exhibiting a fast-spiking phenotype (Figure 3Cg).

MGE- and CGE-Transplant-Derived Interneurons Are Synaptically Integrated

We next tested whether transplanted CGE interneurons become synaptically integrated with host neurons. We again used dual MGE and CGE transplantation from *Nkx2.1-Cre;R26-Ai14;β-actin-GFP* donor embryos, to assess synaptic connectivity between transplant-derived MGE or CGE lineage interneurons and nearby host neurons. Paired intracellular recordings of transplant-derived MGE lineage interneurons and host neurons with large somata and an adapting- or burst-firing pattern (presumed pyramidal neurons) demonstrated postsynaptic responses when presynaptic neurons were driven to threshold by current injection (Figures 4A and 4B). Interneurons derived from MGE transplants made frequent synaptic connections (Figure 4C; six of 20 total connections tested; Figure 4D; inhibitory postsynaptic potential [IPSP] amplitude −0.31 ± 0.07 mV with postsynaptic neuron at −60 mV; Figure 4E; 50-ms paired-pulse ratio 0.7 ± 0.1; Figure 4F; EPSP latency 1.7 ± 0.3 ms, jitter 0.27 ± 0.08 ms). We found a similar connection probability from host pyramidal neurons onto MGE transplant-derived interneurons (Figure 4C; six of 21 connections tested), with EPSP amplitude 1.4 ± 0.4 mV (Figure 4D; with postsynaptic neuron at −70 mV), latency 1.8 ± 0.3 ms (Figure 4F), jitter 0.43 ± 0.07 ms, and a mildly facilitating paired-pulse ratio (Figure 4E; 1.2 ± 0.3, 50-ms interval). This is consistent with prior studies showing that heterochronic MGE transplant-derived interneurons establish frequent connections with nearby pyramidal cells (Southwell et al., 2010) and indicates that the presence of CGE transplant-derived neurons does not disrupt heterochronic integration of MGE transplant-derived neurons.

We next tested whether heterochronically transplanted CGE neurons synapse on local host pyramidal cells and receive synapses from them. In contrast to MGE transplant-derived neurons, connections of pyramidal neurons onto CGE transplant-derived neurons were rare. We only found one connection (out of 15 pairs tested in 14 mice) from a host pyramidal neuron onto a continuously adapting CGE transplant-derived neuron (Figure 5A; Figure S5). The EPSP seen in response to host pyramidal cell firing was similar in amplitude (Figure 5E) to spontaneous EPSPs onto that neuron (1.1 ± 0.7 mV for evoked versus 1.0 ± 0.9 mV for spontaneous, postsynaptic neuron at −70 mV) and was facilitating (Figure 5F; PPR = 1.4), similar to synapses formed by pyramidal neurons onto transplanted MGE-derived neurons. The inverse connection, from CGE transplant-derived interneurons onto host pyramidal cells, was more common

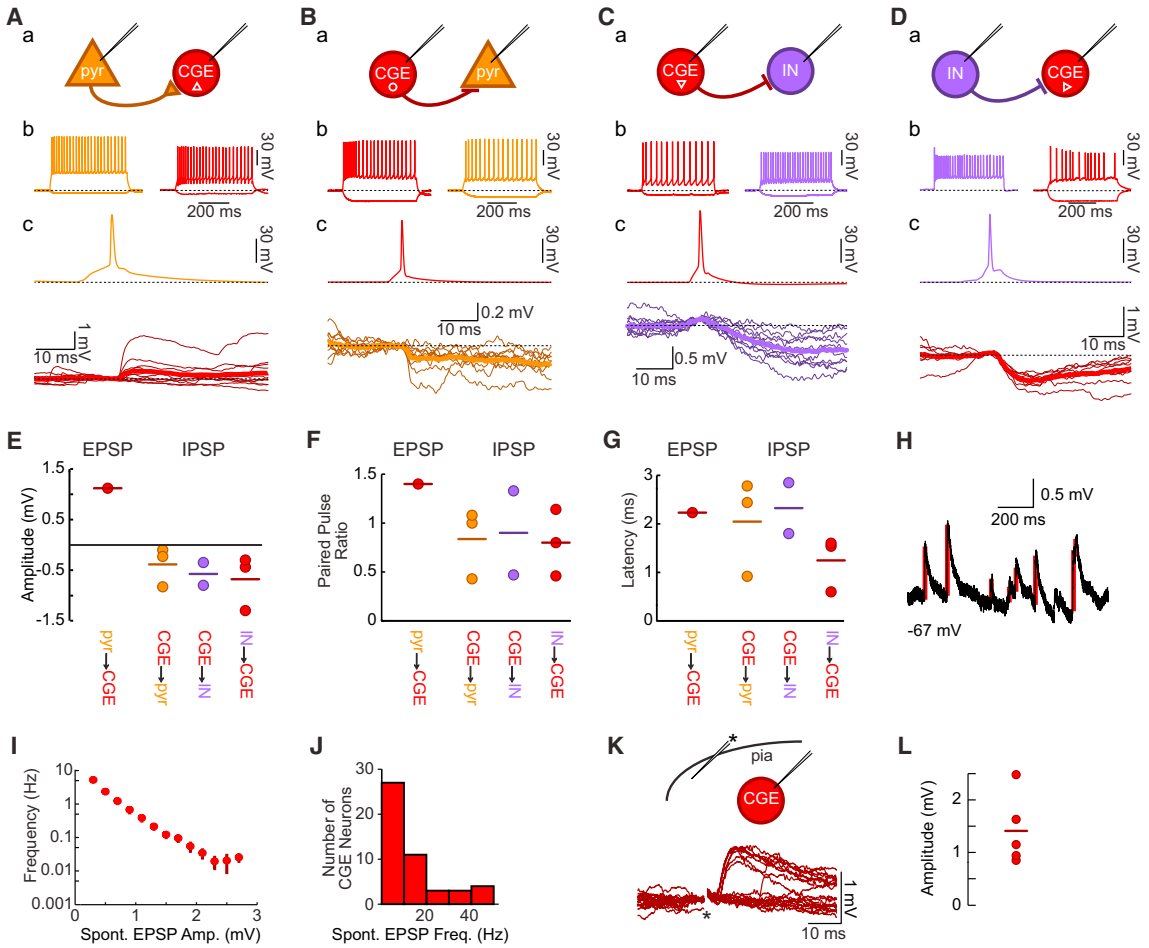

Figure 5. Transplant-Derived CGE Lineage Interneurons Form Functional Synapses with Host Excitatory and Inhibitory Neurons

(A) Whole-cell recordings from a host pyramidal neuron (brown) and a fluorescently labeled transplanted CGE continuous adapting interneuron (red) demonstrate an EPSP onto the postsynaptic CGE-derived neuron (c, bold trace is average of ten responses) when the presynaptic pyramidal neuron fires an action potential (c, brown).

(B) Intracellular recordings from a fluorescently labeled transplanted CGE burst non-adapting non-fast-spiking interneuron (red) and a host pyramidal neuron (brown) demonstrate an IPSP onto the pyramidal neuron following action potentials elicited in the interneuron (c, bold trace is average of ten responses).

(C) Recordings from a fluorescently labeled transplanted CGE continuous non-adapting non-fast-spiking interneuron (*Nkx2.1-Cre;R26-GDTA* donor into an *SST-Cre;R26-Ai14* host; red) and a fluorescently labeled host interneuron (purple) show an IPSP in the host interneuron (c, bold is average of ten responses) following evoked action potentials in the CGE transplant-derived neuron.

(D) Recordings from a host interneuron (*VIP-Cre;R26-Ai14* donor into a *GAD67-GFP* host) show an IPSP onto the transplant-derived CGE lineage continuous irregular firing interneuron (c, bold is average of ten responses).

(E) Quantification of EPSP amplitude from a host pyramidal neuron to a transplant-derived CGE lineage interneuron (red), and IPSP amplitude of transplant-derived CGE lineage interneuron onto host pyramidal neuron (brown), transplant-derived CGE lineage interneuron onto host interneuron (purple), and host interneuron onto transplant-derived CGE lineage interneuron (red).

(F) Quantification of paired-pulse ratios for postsynaptic responses to presynaptic action potentials separated by 50 ms.

(G) Postsynaptic potential onset latency quantifications.

(H) Example trace demonstrating automated EPSP detection (red bars) used in (J) and (K).

(I) Spontaneous EPSPs onto transplanted CGE neurons are small (bar is mean ± SE), though they do also receive infrequent larger inputs (ordinate is logarithmic; n = 16 neurons for which >60 s of spontaneous activity were recorded).

(J) All CGE transplant-derived neurons (n = 48) received spontaneous EPSPs.

(K) Extracellular minimal stimulation in cortical layer I (asterisk) reliably generates EPSPs onto a CGE transplant-derived neuron (amplitude 0.89 ± 0.08 mV for driven versus 0.65 ± 0.41 mV for spontaneous EPSPs, $p > 0.05$). Short latency EPSPs were routinely seen with layer I stimulation (seven of seven CGE neurons tested, latency 4.7 ± 1.3 ms).

(L) Amplitude of EPSP evoked by layer I stimulation with the postsynaptic neuron held at −70 mV (n = 5 neurons, 1.41 ± 0.33 mV).

(Figure 5B; three of 17 connections tested); these connections were typically of small amplitude (Figure 5E; −0.39 ± 0.28 mV, postsynaptic neuron at −60 mV), depressing (Figure 5F; 50 ms PPR = 0.8 ± 0.3), and monosynaptic (Figure 5G; latency: 2.0 ± 0.7 ms, jitter: 0.4 ± 0.1 ms), similar to connections formed by transplanted MGE-derived interneurons ($p > 0.05$ for all comparisons).

Since connections of transplanted CGE interneurons with pyramidal cells were rare, we next investigated whether they establish connections with host interneurons. In order to document connections between transplanted CGE-derived interneurons and host interneurons, we used two transplant strategies, either *Nkx2.1-Cre;R26-GDTA* donors into *SST-Cre;R26-Ai14* hosts (n = 15 connections tested in seven mice) or *VIP-Cre;R26-Ai14* donors into *Gad67-GFP* hosts (n = 9 connections tested in four mice). We found IPSPs in two of 11 tested pairs from CGE transplant-derived neurons to host interneurons (Figure 5C). The IPSPs were small (Figure 5E; −0.58 ± 0.32 mV, postsynaptic neuron at −60 mV), depressing (Figure 5F; 50 ms PPR = 0.9 ± 0.6), and monosynaptic (Figure 5G; latency: 2.3 ± 0.7 ms, jitter: 0.3 ± 0.1 ms). We found the inverse connection (an IPSP from a host interneuron onto a CGE transplant-derived neuron) as well (three of 13 tested connections) and these IPSPs were small (Figure 5E; amplitude: −0.68 ± 0.38 mV), depressing (Figure 5F; 50 ms PPR = 0.8 ± 0.2), and monosynaptic (Figure 5G; latency: 1.2 ± 0.5 ms, jitter: 0.4 ± 0.1 ms).

Both SST^+ and PV^+ MGE-derived interneurons are densely connected to local pyramidal neurons (Fino and Yuste, 2011; Levy and Reyes, 2012), whereas, at least during development, a significant portion of inputs to some CGE-derived neurons (such as RLN^+ neurogliaform cells) arise from distant cortical locations (De Marco García et al., 2015). We found that CGE transplant-derived neurons receive frequent spontaneous excitatory postsynaptic potentials (Figure 5J; IQR 5–15 Hz, via automated detection algorithm demonstrated in Figure 5H). These spontaneous inputs tended to be small, but some larger potentials were also observed (Figure 5I). To elucidate the possible origins of these potentials, we used extracellular stimulation of neurites in layer I of nearby cortex (Figure 5K). This elicited excitatory responses in recorded CGE transplant-derived neurons (Figures 5K and 5L; latency: 4.7 ± 1.3 ms; amplitude: 1.41 ± 0.33 mV). Given that this extracellular stimulation was >500 μm from the soma of the recorded CGE-derived transplanted interneurons, it suggests that the axons stimulated were those of distant neurons. The above data demonstrate that CGE transplant-derived interneurons establish synaptic connections with local excitatory and inhibitory neurons and suggest that a subpopulation of those neurons also receive input from more distant sources. Thus the heterochronically transplanted CGE cells become synaptically connected in a manner that is similar to endogenous CGE-derived interneurons.

CGE Transplanted Cells Are Activated by Visual Stimulation

We next tested whether CGE transplant-derived neurons receive appropriate afferent visual connections. Previous work has shown that VIP neurons respond to visual stimuli and that they play a vital role in adult visual cortex plasticity (Fu et al., 2014, 2015). We used two-photon calcium imaging of awake *VIP-Cre;R26-Ai14* CGE transplant recipients to characterize the responses of transplanted CGE-derived VIP interneurons to visual stimuli (Figure 6A; Figure S6). A calcium sensor was targeted to the transplanted VIP interneurons by injecting a virus containing GCaMP6 (AAV-2/5-CAG-flex-GCaMP6) into the visual cortex at P30, thus allowing Cre-dependent GCaMP6 expression in transplanted VIP interneurons. We found that, similar to host VIP neurons (Fu et al., 2014), roughly half of transplant-derived VIP neurons responded reliably to drifting gratings (Figures 6B, 6D, and 6F; 21 of 37 neurons in two mice), and many of these responses were orientation selective (Figures 6C, 6E, and 6G). These findings suggest that the synaptic inputs to transplant-derived VIP neurons are organized similarly to those of endogenous host VIP neurons.

CGE Transplants Induce ODP, but Not When Depleted of MGE Cells

Previous work has shown that heterochronic transplantation of MGE cells into either neonatal (Southwell et al., 2010) or adult (Davis et al., 2015) mice induces a second period of ocular dominance plasticity. We investigated whether transplantation of CGE cells resulted in plasticity reactivation in the host visual cortex. While a lack of ODP induction was recently reported following CGE transplantation in adult animals, it is unresolved whether this failure in reinstating plasticity is intrinsic to CGE transplants or due to their poor dispersal and aberrant lamination (Davis et al., 2015). Using intrinsic signal optical imaging, we first tested recipients of *R26-GDTA* MGE and CGE cells for plasticity at 33–35 DAT, when MGE cells display the greatest ability to induce plasticity (Figure 7A; Southwell et al., 2010). Following 4–5 days of monocular deprivation, MGE and CGE transplants induced robust plasticity as indicated by a shift in ocular dominance index (ODI; Figure 7B; n = 6 mice for MGE, n = 9 mice for CGE; Mann-Whitney $p < 0.01$, $p < 0.001$). Amplitude of the ODI shift was indistinguishable between MGE and CGE transplants (Figure 7C; $p > 0.05$). We analyzed the changes in magnitude of the visual cortical responses for each eye and found that both MGE and CGE transplant-induced plasticity included the depression of responses to stimulation of the deprived contralateral eye that is characteristic of critical period plasticity (Figure 7D).

Because anatomically isolated CGE transplants contain a small population of MGE-derived PV and SST interneuron contaminants (Figure 1 and Figures 7F and 7G, magenta), we next asked whether these MGE cells could account for the observed plasticity in CGE transplant recipients. We selectively ablated MGE-derived PV and SST cells from our CGE transplants by crossing *R26-GDTA* and *PV-Cre;SST-Cre* mice. In agreement with our initial characterization of these transplants (Figure 2H), we found that the visual cortex of *PV-Cre;SST-Cre;R26-GDTA* E13.5 CGE recipients contained virtually no transplanted PV and SST cells at 35 DAT (Figures 7F and 7G, red). MD failed to induce plasticity in these animals (Figure 7B, red; n = 7 mice; Mann-Whitney $p > 0.05$), and they exhibited no significant ODI shift, significantly different from that of *R26-GDTA* MGE or CGE recipients (Figure 7C; Bonferroni-corrected Mann-Whitney $p < 0.01$ versus MGE group, $p < 0.001$ versus CGE group). A

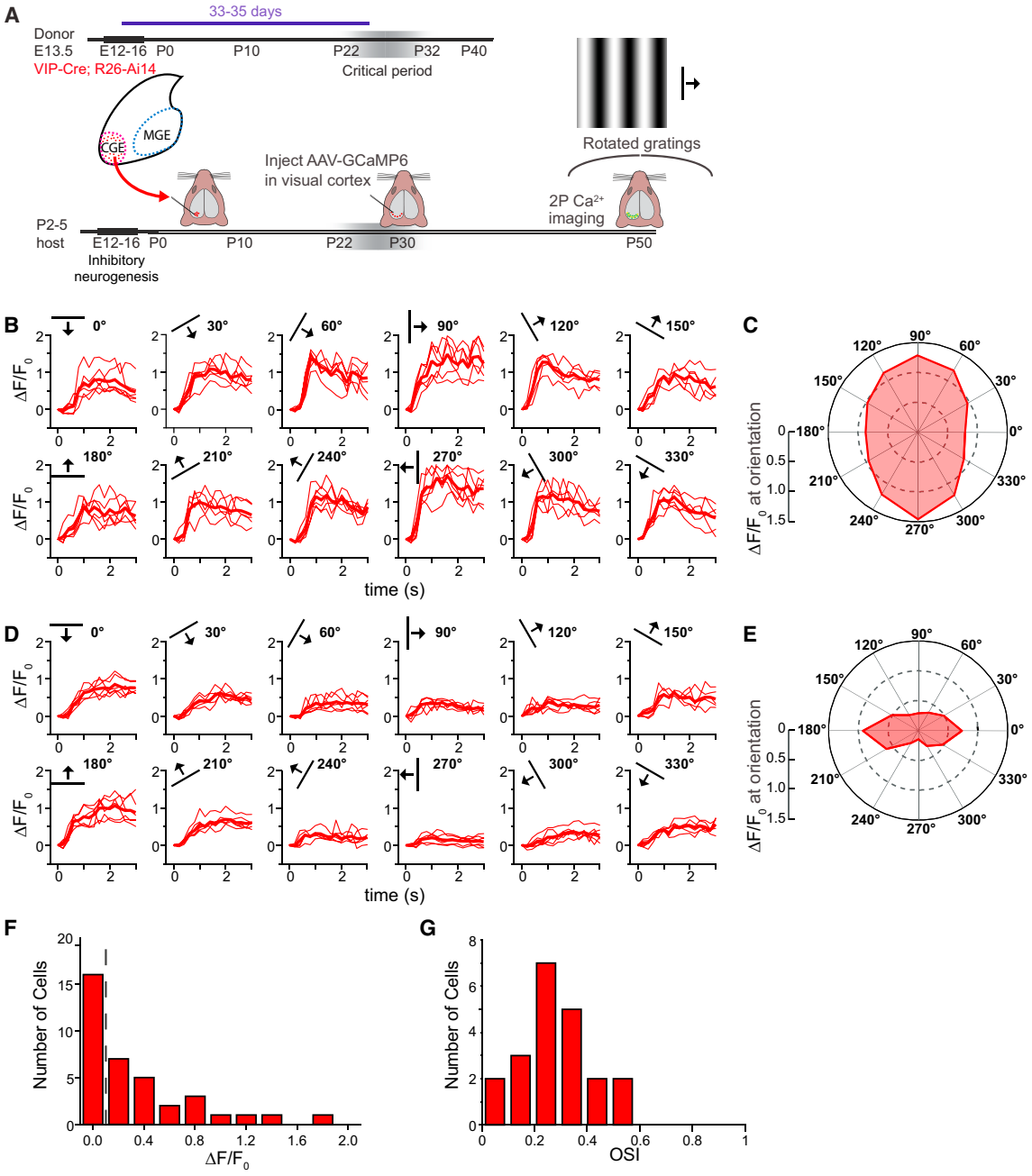

Figure 6. Activity in CGE Transplant-Derived VIP-Expressing Interneurons Is Visually Modulated

(A) Donor CGE tissue (*VIP-Cre;R26-Ai14*) was harvested at E13.5 and transplanted at P7 into wild-type hosts. AAV-2/5-CAG-flex-GCaMP6s was injected into visual cortex at P30 and in vivo two photon calcium responses to rotated drifting gratings were obtained 3 weeks later in transplant-derived neurons (tdTomato^{+}).

(B) Calcium responses of a transplanted VIP neuron to drifting gratings (orientation indicated by bar in upper left). Red traces represent individual trials and bold trace is the average of six trials ($\Delta F/F_0$ at preferred orientation = 1.46).

(C) Polar chart of the response in (B), averaged over the last 2 s of the stimulus period, demonstrates broad tuning (OSI = 0.21).

(D) A second exemplar neuron with $\Delta F/F_0$ = 0.88 at preferred orientation.

(E) Polar chart of the averaged response in (D) demonstrates narrow orientation tuning for this neuron (OSI = 0.54).

(F) Distribution of average response magnitudes at the preferred orientation in all cells analyzed (n = 37 cells in two mice). Responses greater than 0.1 (dashed line) were considered visually responsive.

(G) Distribution of orientation selectivity in visually responsive cells (n = 21 cells in two mice).

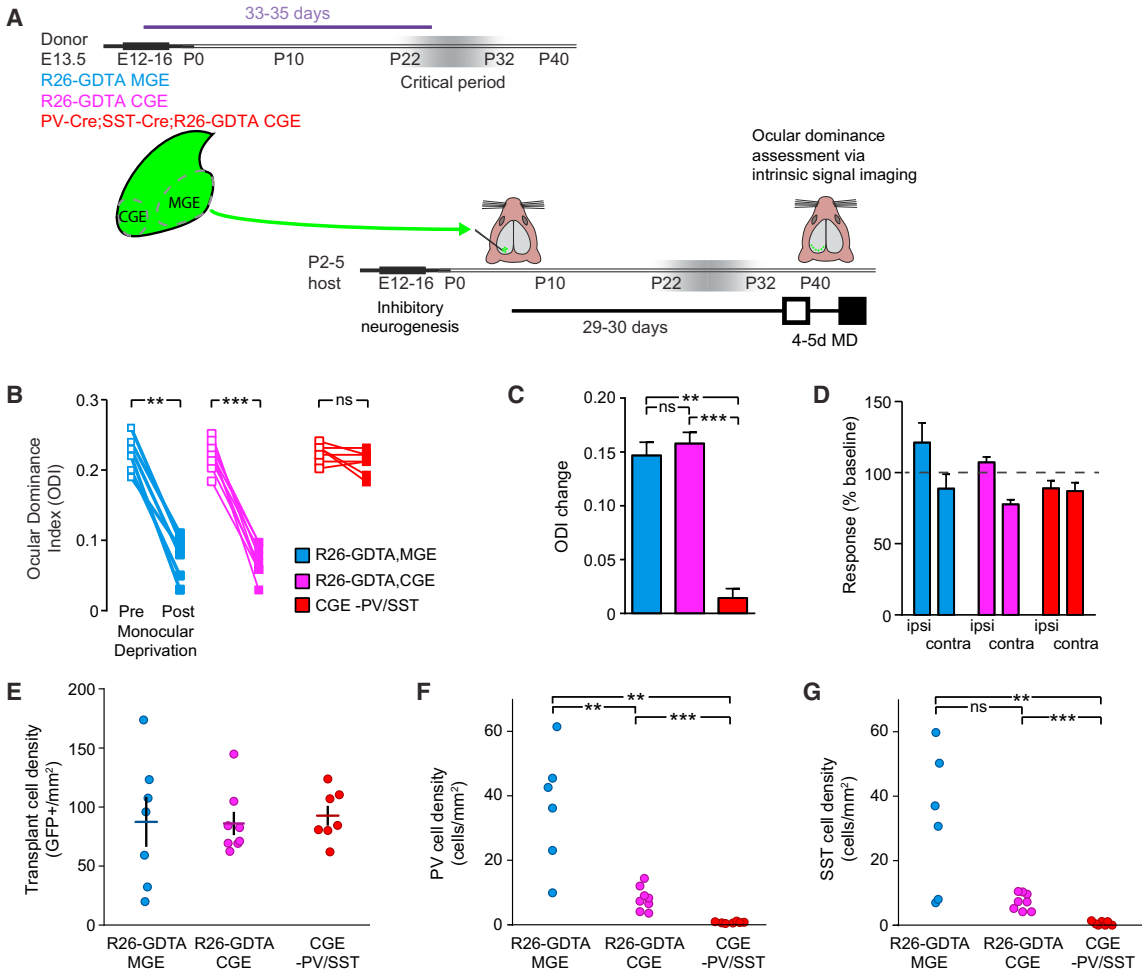

Figure 7. Genetically Purified CGE Transplants Do Not Induce a Heterochronic Critical Period

(A) *R26-GDTA* MGE (blue), *R26-GDTA* CGE (magenta), or *PV-Cre;SST-Cre;R26-GDTA* CGE cells (red) were harvested at E13.5, dissociated, and transplanted into the visual cortex of P7 hosts. Animals were imaged before and after a 4- to 5-day period of monocular deprivation starting at 29–30 DAT.

(B) Ocular dominance index measured before (open squares) and after (closed squares) 4–5 days of monocular deprivation of the contralateral eye demonstrate significant plasticity in MGE (blue, n = 6) and CGE (magenta, n = 9) cell transplant recipients. Ocular dominance index for PV- and SST-depleted CGE transplants (*PV-Cre;SST-Cre;R26-GDTA*, red, n = 7) do not demonstrate significant plasticity (no change in ODI, $p > 0.05$). Significance calculated using Bonferroni-corrected Mann-Whitney tests.

(C) Magnitude of ODI change following deprivation. Significance calculated using Bonferroni-corrected Mann-Whitney tests.

(D) Changes in magnitude of ipsilateral and contralateral responses after deprivation, expressed as percentage of pre-MD baseline values (dashed line).

(E) Density of GFP-expressing transplanted cells in the binocular visual cortex of recipients of MGE (blue, n = 6), CGE (magenta, n = 8) and PV-SST-depleted CGE (red, n = 7) cell transplants, at 35 DAT. Horizontal bars represent mean and vertical bars SEM.

(F) Density of transplanted PV cells in host binocular visual cortex.

(G) Density of transplanted SST cells in host binocular visual cortex. Significance calculated using Bonferroni-corrected Mann-Whitney test.

similar lack of ODP induction was found following transplants of *Nkx2.1-Cre;R26-GDTA* donor CGE cells in which MGE-derived cells are ablated early in development (Figure S7; n = 3 mice). Total transplant-derived neuron density in the visual cortex of *PV-Cre;SST-Cre;R26-GDTA* CGE recipients was similar to that of *R26-GDTA* MGE and *R26-GDTA* CGE recipients (Figure 7E), despite successful ablation of PV- (Figure 7F) and SST (Figure 7G)-expressing neurons from those transplants. Taken together, our results demonstrate that MGE-derived PV and SST interneurons play a unique role in transplant induced ODP, while genetically purified CGE transplant-derived interneurons, despite being functionally integrated, do not induce similar plasticity.

DISCUSSION

Our data demonstrate that transplanted interneurons derived from CGE progenitors can migrate broadly, integrate into the host visual cortex, and retain their lineage-specific fate, as measured using anatomical location, marker expression, electrophysiology, and calcium imaging of visual responses in awake mice. However, despite successful engraftment into the host

visual cortex, CGE transplants induce ODP only if they contain MGE-derived PV and SST interneurons. This demonstrates the unique requirement of MGE-derived PV and SST interneurons for the induction of plasticity. Of course, CGE-derived interneurons are key elements in the cortical circuit and may facilitate the ability of MGE cells to induce plasticity, but pure transplants of CGE neurons, without co-transplanting MGE neurons, do not. As with the MGE transplantation, the dispersion and integration of heterochronically grafted CGE cells offers a powerful experimental tool to investigate what their functional contributions to cortical circuits are.

Consistent with previous lineage tracing studies (Lee et al., 2010; Miyoshi et al., 2010; Rudy et al., 2011; Vucurovic et al., 2010), CGE-derived interneurons were more likely, compared to MGE-derived interneurons, to populate layer I and predominantly expressed VIP, CR, or RLN. Further, our data indicate that the few transplanted PV and SST interneurons found in the brain of CGE recipients were derived from the MGE, consistent with the known developmental origin of PV and SST cells (Butt et al., 2005; Nery et al., 2002; Wichterle et al., 1999, 2001; Xu et al., 2008).

CGE-derived interneurons displayed a diverse array of intrinsic electrophysiological properties, consistent with studies of CGE-lineage neurons (Lee et al., 2010; Vucurovic et al., 2010). They demonstrated synaptic connections to host inhibitory neurons and appear to be sparsely innervated by local pyramidal neurons, similar to what has been observed for endogenous CGE lineage VIP cells (Pfeffer et al., 2013). Finally, CGE transplant-derived VIP-expressing interneurons show orientation selectivity similar to that seen in endogenous VIP neurons (Fu et al., 2014). This provides further evidence that these neurons become synaptically integrated into host cortex. These findings, in conjunction with data from MGE transplant-derived interneurons (Figures 1, 2, 3, and 4; Davis et al., 2015; Southwell et al., 2010), show that transplantation of different subsets of ganglionic eminence cells produces genetically and physiologically defined subsets of mature interneurons that are functionally integrated into host cortical circuits.

In our physiological recordings we identified one neuron with a fast-spiking phenotype. This is surprising given that prior characterization of the CGE lineage at a juvenile time point using either a Mash1-promoter-driven label (Miyoshi et al., 2010) or the 5HT3aR (Lee et al., 2010) did not identify fast-spiking interneurons. One possible explanation for these findings is the well-characterized maturation of interneuron spiking in juvenile mice. Even PV-expressing interneurons, for which a fast-spiking phenotype is characteristic once mature, are not fast spiking during juvenile time periods (Okaty et al., 2009). Comparable studies on the maturation of CGE lineage neurons are not currently available and may reveal that a fast-spiking phenotype in adulthood is consistent with that lineage.

We observed a relatively high proportion of RLN neurons (39%) in our CGE-derived transplants compared to the normal proportion of endogenous RLN neurons (24%; Lee et al., 2010). RLN neurons' survival is critically dependent on activity (De Marco García et al., 2011). It is possible that our heterochronically grafted CGE-derived interneurons are exposed during their maturation to higher levels of activity compared to the normal course of development. Alternatively, the higher proportion of RLN interneurons in our transplants could be explained by CGE dissections that were limited to the caudal dorsal CGE. Previous work has suggested that the dorsal and ventral CGE produce distinct distributions of neuron types (Butt et al., 2005). The preponderance of our CGE transplant-derived neurons exhibited the continuous adapting spiking phenotype, which is typical for RLN neurons and the subset of layer I neurogliaform neurons from which we recorded demonstrated late spiking at rheobase. These factors, combined with the appropriate laminar preference and neurogliaform morphology of our transplant-derived RLN neurons, suggest that RLN neurons do differentiate and mature appropriately.

While previous groups have reported limited migration and aberrant lamination of transplanted CGE cells in the adult visual cortex (Davis et al., 2015), our CGE transplants into juvenile cortex exhibited lamination reminiscent of the CGE lineage and were indistinguishable from MGE transplants in the extent of their dispersal in the host brain. These differences could be explained by the age of the recipients, as migration and engraftment may be facilitated in the neonatal brain where myelin and extracellular matrix are still underdeveloped. Further, we find that CGE transplants contaminated with even a small (~10%) population of MGE-derived PV and SST cells do allow induction of robust ODP, consistent with prior work showing plasticity induction with similar transplant-derived MGE lineage interneuron densities (Southwell et al., 2010; Tang et al., 2014), and thus demonstrating that the presence of CGE-derived interneurons does not impair ODP induction.

Conversely, although CGE transplant-derived neurons demonstrated normal phenotypes and integrated into host circuits appropriately, they did not allow heterochronic induction of ODP. The maturation of endogenous interneurons is tightly associated with the induction of endogenous ODP (Espinosa and Stryker, 2012). Similarly, transplant-induced ODP depends on the maturation of interneurons in the heterochronic environment. However, the lack of ODP in CGE recipients shows that the mechanisms required for cellular and synaptic integration of the transplants are not sufficient to induce critical period plasticity.

Furthermore, as CGE-derived interneurons are synaptically connected to nearby neurons, the increased plasticity seen following MGE cell transplant is not likely to be due to homeostatic compensation for a diffuse increase in inhibitory tone. Rather, that CGE transplantation does not allow ODP suggest that MGE lineage neurons play a unique role in ocular dominance plasticity, either through their specific synaptic connections or via a secreted factor that is unique to MGE lineage neurons. This implies that separate neuron types support juvenile/developmental versus adult cortical plasticity and will thus help to focus future studies into the molecular and synaptic mechanisms underlying such plasticity.

EXPERIMENTAL PROCEDURES

Animals

R26-Ai14, β-actin-GFP, Gad67-GFP, Nkx2.1-Cre, SST-Cre, PV-Cre, VIP-Cre, R26-GDTA, and wild-type C57BL/6J breeders were purchased from The

Jackson Laboratory. All protocols and procedures followed University of California, San Francisco (UCSF) guidelines and were approved by the UCSF Institutional Animal Care and Use Committee.

Cell Dissection and Transplantation

MGE and/or CGE were dissected from E13.5–E14.5 donor embryos, mechanically dissociated, concentrated via centrifugation (800 × *g* for 3 min), and injected into P5–8 recipient mice.

Immunostaining

Floating 40-μm sections were created after perfusion and fixation. They were blocked, incubated with primary antibodies, washed, incubated with Alexa-conjugated secondary antibodies, and then washed again prior to coverslipping.

Cell Counting

Cell density was defined as the number of fluorescent cells within the binocular visual cortex divided by the total area as identified functionally during intrinsic signal imaging sessions.

Intrinsic Signal Imaging

Animals were anesthetized with isoflurane/chlorprothixene, and ISI was performed and ODI was calculated using standard Fourier methods (Kalatsky and Stryker, 2003).

Calcium Imaging

At P30, AAV-2/5-CAG-flex-GCaMP6s was injected stereotaxically into primary visual cortex (V1) of mice transplanted at P2 with *VIP-Cre* and *R26-Ai14* donor CGE. Three weeks after virus injection, a craniotomy was created over V1 and covered with a glass coverslip. Calcium signals were recorded from identified neurons 150–300 μm below the cortical surface at 5 Hz (using a custom modified two-photon microscope) during presentation of drifting sinusoidal gratings presented in 12 different orientations. Neurons were considered visually responsive when $\Delta F/F_o$, averaged over the last 2 s of visual stimulation was significantly related to the stimulus by ANOVA and average $\Delta F/F_o$ at preferred orientations was greater than 10%. The orientation selectivity index (OSI) was computed for responsive cells as:

$$\frac{\sqrt{\left(\sum R(\theta_i) * \sin(2\theta_i)\right)^2 + \left(\sum R(\theta_i) * \cos(2\theta_i)\right)^2}}{\sum R(\theta_i)}$$

where θ_i is the orientation of each stimulus and $R(\theta_i)$ is the response to that stimulus (Fu et al., 2014).

Electrophysiology

Recordings were made at P35–43 from fluorescently identified host or donor neurons in coronal V1 slices. Synaptic connectivity and neuron intrinsic physiological properties were assessed via intracellular current injections.

Statistics

Statistical tests are stated separately for each comparison. Significance is indicated on figures as follows: ns, not significant, *$p < 0.05$, **$p < 0.01$, ***$p < 0.001$.

SUPPLEMENTAL INFORMATION

Supplemental Information includes Supplemental Experimental Procedures and seven figures and can be found with this article online at http://dx.doi.org/10.1016/j.celrep.2016.06.071.

AUTHOR CONTRIBUTIONS

P.L., J.S., J.S.E., Y.T., A.H., M.P.S., and A.A.-B. designed the experiments. J.S. and Y.T. performed the transplantation procedures and histological analyses. J.S.E. and M.K. performed intrinsic signal and calcium imaging experiments. P.L. performed intracellular recordings. P.L., J.S., Y.T., A.H., M.P.S., and A.A.-B wrote the manuscript.

ACKNOWLEDGMENTS

This work was supported by the California Institute for Regenerative Medicine Grant TG2-01153 (to A.A.-B.); NIH grants R01EY025174 (to A.A.-B. and M.P.S.), R01EY02874 (to M.P.S.), R01DC014101 (to A.H.), T32GM007618 (to Y.T.), R25NS070680 (to P.L.), and K22NS089799 (to J.S.E.) and a University of California President's Postdoctoral Fellowship Program Grant (to J.S.E.). M.P.S. is the recipient of the RPB Stein Innovation Award. A.A.-B is the Heather and Melanie Muss Endowed Chair.

Received: January 13, 2016
Revised: May 4, 2016
Accepted: June 16, 2016
Published: July 14, 2016

REFERENCES

Alvarez-Dolado, M., Calcagnotto, M.E., Karkar, K.M., Southwell, D.G., Jones-Davis, D.M., Estrada, R.C., Rubenstein, J.L.R., Alvarez-Buylla, A., and Baraban, S.C. (2006). Cortical inhibition modified by embryonic neural precursors grafted into the postnatal brain. J. Neurosci. *26*, 7380–7389.

Anderson, S.A., Eisenstat, D.D., Shi, L., and Rubenstein, J.L. (1997). Interneuron migration from basal forebrain to neocortex: dependence on Dlx genes. Science *278*, 474–476.

Arlotta, P., Molyneaux, B.J., Chen, J., Inoue, J., Kominami, R., and Macklis, J.D. (2005). Neuronal subtype-specific genes that control corticospinal motor neuron development in vivo. Neuron *45*, 207–221.

Ascoli, G.A., Alonso-Nanclares, L., Anderson, S.A., Barrionuevo, G., Benavides-Piccione, R., Burkhalter, A., Buzsáki, G., Cauli, B., Defelipe, J., Fairén, A., et al.; Petilla Interneuron Nomenclature Group (2008). Petilla terminology: nomenclature of features of GABAergic interneurons of the cerebral cortex. Nat. Rev. Neurosci. *9*, 557–568.

Bráz, J.M., Sharif-Naeini, R., Vogt, D., Kriegstein, A., Alvarez-Buylla, A., Rubenstein, J.L., and Basbaum, A.I. (2012). Forebrain GABAergic neuron precursors integrate into adult spinal cord and reduce injury-induced neuropathic pain. Neuron *74*, 663–675.

Britanova, O., de Juan Romero, C., Cheung, A., Kwan, K.Y., Schwark, M., Gyorgy, A., Vogel, T., Akopov, S., Mitkovski, M., Agoston, D., et al. (2008). Satb2 is a postmitotic determinant for upper-layer neuron specification in the neocortex. Neuron *57*, 378–392.

Butt, S.J.B., Fuccillo, M., Nery, S., Noctor, S., Kriegstein, A., Corbin, J.G., and Fishell, G. (2005). The temporal and spatial origins of cortical interneurons predict their physiological subtype. Neuron *48*, 591–604.

Chattopadhyaya, B., Di Cristo, G., Higashiyama, H., Knott, G.W., Kuhlman, S.J., Welker, E., and Huang, Z.J. (2004). Experience and activity-dependent maturation of perisomatic GABAergic innervation in primary visual cortex during a postnatal critical period. J. Neurosci. *24*, 9598–9611.

Davis, M.F., Figueroa Velez, D.X., Guevarra, R.P., Yang, M.C., Habeeb, M., Carathedathu, M.C., and Gandhi, S.P. (2015). Inhibitory neuron transplantation into adult visual cortex creates a new critical period that rescues impaired vision. Neuron *86*, 1055–1066.

De Marco García, N.V., Karayannis, T., and Fishell, G. (2011). Neuronal activity is required for the development of specific cortical interneuron subtypes. Nature *472*, 351–355.

De Marco García, N.V., Priya, R., Tuncdemir, S.N., Fishell, G., and Karayannis, T. (2015). Sensory inputs control the integration of neurogliaform interneurons into cortical circuits. Nat. Neurosci. *18*, 393–401.

Espinosa, J.S., and Stryker, M.P. (2012). Development and plasticity of the primary visual cortex. Neuron *75*, 230–249.

Fino, E., and Yuste, R. (2011). Dense inhibitory connectivity in neocortex. Neuron *69*, 1188–1203.

Fishell, G., and Tamás, G. (2014). Inhibition: synapses, neurons and circuits. Curr. Opin. Neurobiol. *26*, v–vii.

Fu, Y., Tucciarone, J.M., Espinosa, J.S., Sheng, N., Darcy, D.P., Nicoll, R.A., Huang, Z.J., and Stryker, M.P. (2014). A cortical circuit for gain control by behavioral state. Cell *156*, 1139–1152.

Fu, Y., Kaneko, M., Tang, Y., Alvarez-Buylla, A., and Stryker, M.P. (2015). A cortical disinhibitory circuit for enhancing adult plasticity. eLife *4*, e05558.

Gibson, J.R., Beierlein, M., and Connors, B.W. (1999). Two networks of electrically coupled inhibitory neurons in neocortex. Nature *402*, 75–79.

Hensch, T.K. (2005). Critical period plasticity in local cortical circuits. Nat. Rev. Neurosci. *6*, 877–888.

Hippenmeyer, S., Vrieseling, E., Sigrist, M., Portmann, T., Laengle, C., Ladle, D.R., and Arber, S. (2005). A developmental switch in the response of DRG neurons to ETS transcription factor signaling. PLoS Biol. *3*, e159.

Hunt, R.F., Girskis, K.M., Rubenstein, J.L., Alvarez-Buylla, A., and Baraban, S.C. (2013). GABA progenitors grafted into the adult epileptic brain control seizures and abnormal behavior. Nat. Neurosci. *16*, 692–697.

Ivanova, A., Signore, M., Caro, N., Greene, N.D.E., Copp, A.J., and Martinez-Barbera, J.P. (2005). In vivo genetic ablation by Cre-mediated expression of diphtheria toxin fragment A. Genesis *43*, 129–135.

Kalatsky, V.A., and Stryker, M.P. (2003). New paradigm for optical imaging: temporally encoded maps of intrinsic signal. Neuron *38*, 529–545.

Kawaguchi, Y., and Kubota, Y. (1997). GABAergic cell subtypes and their synaptic connections in rat frontal cortex. Cereb. Cortex *7*, 476–486.

Lee, S., Hjerling-Leffler, J., Zagha, E., Fishell, G., and Rudy, B. (2010). The largest group of superficial neocortical GABAergic interneurons expresses ionotropic serotonin receptors. J. Neurosci. *30*, 16796–16808.

Levy, R.B., and Reyes, A.D. (2012). Spatial profile of excitatory and inhibitory synaptic connectivity in mouse primary auditory cortex. J. Neurosci. *32*, 5609–5619.

Ma, Y., Hu, H., Berrebi, A.S., Mathers, P.H., and Agmon, A. (2006). Distinct subtypes of somatostatin-containing neocortical interneurons revealed in transgenic mice. J. Neurosci. *26*, 5069–5082.

Madisen, L., Zwingman, T.A., Sunkin, S.M., Oh, S.W., Zariwala, H.A., Gu, H., Ng, L.L., Palmiter, R.D., Hawrylycz, M.J., Jones, A.R., et al. (2010). A robust and high-throughput Cre reporting and characterization system for the whole mouse brain. Nat. Neurosci. *13*, 133–140.

Maffei, A., Nataraj, K., Nelson, S.B., and Turrigiano, G.G. (2006). Potentiation of cortical inhibition by visual deprivation. Nature *443*, 81–84.

Martínez-Cerdeño, V., Noctor, S.C., Espinosa, A., Ariza, J., Parker, P., Orasji, S., Daadi, M.M., Bankiewicz, K., Alvarez-Buylla, A., and Kriegstein, A.R. (2010). Embryonic MGE precursor cells grafted into adult rat striatum integrate and ameliorate motor symptoms in 6-OHDA-lesioned rats. Cell Stem Cell *6*, 238–250.

Miyoshi, G., Hjerling-Leffler, J., Karayannis, T., Sousa, V.H., Butt, S.J.B., Battiste, J., Johnson, J.E., Machold, R.P., and Fishell, G. (2010). Genetic fate mapping reveals that the caudal ganglionic eminence produces a large and diverse population of superficial cortical interneurons. J. Neurosci. *30*, 1582–1594.

Nery, S., Fishell, G., and Corbin, J.G. (2002). The caudal ganglionic eminence is a source of distinct cortical and subcortical cell populations. Nat. Neurosci. *5*, 1279–1287.

Okaty, B.W., Miller, M.N., Sugino, K., Hempel, C.M., and Nelson, S.B. (2009). Transcriptional and electrophysiological maturation of neocortical fast-spiking GABAergic interneurons. J. Neurosci. *29*, 7040–7052.

Pfeffer, C.K., Xue, M., He, M., Huang, Z.J., and Scanziani, M. (2013). Inhibition of inhibition in visual cortex: the logic of connections between molecularly distinct interneurons. Nat. Neurosci. *16*, 1068–1076.

Pizzorusso, T., Medini, P., Berardi, N., Chierzi, S., Fawcett, J.W., and Maffei, L. (2002). Reactivation of ocular dominance plasticity in the adult visual cortex. Science *298*, 1248–1251.

Prönneke, A., Scheuer, B., Wagener, R.J., Möck, M., Witte, M., and Staiger, J.F. (2015). Characterizing VIP Neurons in the Barrel Cortex of VIPcre/tdTomato Mice Reveals Layer-Specific Differences. Cereb. Cortex *25*, 4854–4868.

Reyes, A., Lujan, R., Rozov, A., Burnashev, N., Somogyi, P., and Sakmann, B. (1998). Target-cell-specific facilitation and depression in neocortical circuits. Nat. Neurosci. *1*, 279–285.

Rudy, B., Fishell, G., Lee, S., and Hjerling-Leffler, J. (2011). Three groups of interneurons account for nearly 100% of neocortical GABAergic neurons. Dev. Neurobiol. *71*, 45–61.

Southwell, D.G., Froemke, R.C., Alvarez-Buylla, A., Stryker, M.P., and Gandhi, S.P. (2010). Cortical plasticity induced by inhibitory neuron transplantation. Science *327*, 1145–1148.

Sussel, L., Marin, O., Kimura, S., and Rubenstein, J.L. (1999). Loss of Nkx2.1 homeobox gene function results in a ventral to dorsal molecular respecification within the basal telencephalon: evidence for a transformation of the pallidum into the striatum. Development *126*, 3359–3370.

Tang, Y., Stryker, M.P., Alvarez-Buylla, A., and Espinosa, J.S. (2014). Cortical plasticity induced by transplantation of embryonic somatostatin or parvalbumin interneurons. Proc. Natl. Acad. Sci. USA *111*, 18339–18344.

Taniguchi, H., He, M., Wu, P., Kim, S., Paik, R., Sugino, K., Kvitsiani, D., Fu, Y., Lu, J., Lin, Y., et al. (2011). A resource of Cre driver lines for genetic targeting of GABAergic neurons in cerebral cortex. Neuron *71*, 995–1013.

Vucurovic, K., Gallopin, T., Ferezou, I., Rancillac, A., Chameau, P., van Hooft, J.A., Geoffroy, H., Monyer, H., Rossier, J., and Vitalis, T. (2010). Serotonin 3A receptor subtype as an early and protracted marker of cortical interneuron subpopulations. Cereb. Cortex *20*, 2333–2347.

Wichterle, H., Garcia-Verdugo, J.M., Herrera, D.G., and Alvarez-Buylla, A. (1999). Young neurons from medial ganglionic eminence disperse in adult and embryonic brain. Nat. Neurosci. *2*, 461–466.

Wichterle, H., Turnbull, D.H., Nery, S., Fishell, G., and Alvarez-Buylla, A. (2001). In utero fate mapping reveals distinct migratory pathways and fates of neurons born in the mammalian basal forebrain. Development *128*, 3759–3771.

Wonders, C.P., and Anderson, S.A. (2006). The origin and specification of cortical interneurons. Nat. Rev. Neurosci. *7*, 687–696.

Xu, Q., Tam, M., and Anderson, S.A. (2008). Fate mapping Nkx2.1-lineage cells in the mouse telencephalon. J. Comp. Neurol. *506*, 16–29.

Zipancic, I., Calcagnotto, M.E., Piquer-Gil, M., Mello, L.E., and Alvarez-Dolado, M. (2010). Transplant of GABAergic precursors restores hippocampal inhibitory function in a mouse model of seizure susceptibility. Cell Transplant. *19*, 549–564.